

Commuting Conditional GANs for Robust Multi-Modal Fusion

Siddharth Roheda*, Hamid Krim*, and Benjamin S. Riggan†.

*North Carolina State University at Raleigh, NC, USA

†University of Nebraska-Lincoln, Lincoln, NE, USA

Abstract—This paper presents a data driven approach to multi-modal fusion, where optimal features for each sensor are selected from a common hidden space between the different modalities. The existence of such a hidden space is then used in order to detect damaged sensors and safeguard the performance of the system. Experimental results show that such an approach can make the system robust against noisy/damaged sensors, without requiring human intervention to inform the system about the damage.

I. INTRODUCTION

IN recent years, multi-modal fusion has attracted a lot of research interest, both in academia, and in the industry. Multi-modal fusion involves combining information from multiple sources. In particular, target detection and recognition problems have widely used a multi-modal approach in order to boost performance of detection systems. Different sensors may provide different information about the target, and hence, a system combining the information from multiple sensors is expected to lead to better performance compared to one that relies on information from an individual sensor. Such a fusion of sensor data requires some kind of principled technique, in order to ensure that additional data is used constructively, and has a positive impact on performance. Sensor fusion is known to broadly classify fusion techniques into three classes. Data level fusion is used when one wishes to combine raw data, and then proceed with inference. Feature level fusion first extracts information from raw data, and then merges these features to make coherent decisions. Finally, the latest point at which one can perform fusion is known as decision level fusion. Fusion on the decision level allows each sensor to reach to an individual decision (on the target identity) prior to optimal combination of these decisions.

Decision level fusion has received a lot of attention when it comes to dealing with heterogeneous modalities, as it allows each modality to have a separate feature representation, capturing the additional information that it provides. A review of existing fusion approaches can be seen in [1], [2]. Over the years, classical techniques like Bayesian Fusion [3], and Dempster-Shafer Fusion [4] have been widely used to combine sensor modalities at the decision level. While, more recent approaches include a model based fusion technique [5], [6], [7], which models a network of sensors to be made up of similar or dissimilar sensors. Similar Sensor Fusion [5], [6] is used when all sensors explore the same characteristics of the target, while Dissimilar Sensor Fusion [5], [7] is used

when sensors observe different characteristics of the target, and hence provide new information about the target. Another framework for fusion is presented in [8], [9], which reaches a classification decision by cataloging sets of events, along with their probabilistic characterization for each sensor, and following a joint probabilistic and coherent evaluation of these events. These events are formalized to each sensor according to its potentially extracted attributes to define targets. This leads to a probability measure assignment to a specific target following its description. The major drawback with this framework is that the features are hand-crafted, and so are the target defining events. This makes classification/fusion difficult when the high level features (eg. velocity, weight, etc.) of the targets are unknown.

In fusion applications, a major hurdle is ensuring that all the sensors contributing towards the fusion are reliable, i.e. none of them is damaged and transmitting garbage values to the fusion system, leading to erroneous decisions. This becomes extremely important in unconstrained surveillance settings where the environmental conditions have a direct impact on the sensors, and regular checks by humans may not be possible. This usually causes a major drop in performance of the fusion system if not detected and dealt with. Furthermore, even if these sensors are detected successfully, the common approach to deal with them is to ignore the damaged sensor, with a potential negative impact on the performance relative to the ideal scenario (i.e. when all sensors are functional). We consider exploiting the prior information about the relationship between these sensor modalities, so that the fusion system can safeguard a high performance. This prior information is obtained from the past observations of the damaged sensor which were available during the training of the fusion model. Recently there has been an interest in such a transfer of knowledge. In [10], the authors introduce hallucination networks that address a missing modality at test time by distilling knowledge into the network during training. Here, a teacher-student network is implemented using an L^2 loss term (hallucination loss) to train the student network. This idea has been further extended in [11], [12], [13]. In [13] a Conditional Generative Adversarial Network (CGAN) was used to generate representative features for the missing modality. Furthermore, [14] shows that considering interactions between modalities can often lead to a better feature representation. Recent work in Domain Adaptation [15], [16], [17] addresses differences between source and target domains. In these works, the authors attempt to learn intermediate domains (represented as points

on the Grassman manifold in [15], [16] and by dictionaries in [17]) between the source domain and the target domain.

Our Contributions: In this paper, we propose a robust sensor fusion algorithm, that can detect damaged sensors on the fly and take the required steps to safeguard detection performance. We use a special case of the Event Driven Fusion technique recently proposed in [8], [9], and modify it in order to include reliability of individual sensors. This reliability measure is adaptive, and accounts for the sensor condition during implementation. We also propose a data driven approach for learning the features of interest which were handcrafted in [8]. In addition, we learn a hidden latent space between the sensor modalities and the optimal features for classification are driven by the existence of this hidden space. Furthermore, it also provides robustness against damaged sensors. This hidden space is learned via a generative network conditioned on individual sensor modalities. Unlike [13], we do not require any target feature space in order to learn the optimal hidden space estimates. The hidden space is structured so that it can accommodate both shared and private features of sensor modalities. Unlike [9], we do not need to assume a-priori knowledge about sensor damage, and can detect damaged sensors based on deviations in the generated hidden space.

II. RELATED WORK

A. Model Based Sensor Fusion

1) Similar Sensor Fusion: This model for sensor fusion assumes that independent sensors in the network are similar to each other (eg. 5 radars looking at the same object). Additional sensors in this case do not provide any new information, but can be used to confirm information from other sensors. This model attempts to find a fusion result which is most consistent with all the individual sensor reports. Given a set of objects/targets, $O = \{o_1, o_2, \dots, o_I\}$, the l^{th} sensor report is defined as $R^l = \{P^l(o_i)\}$. In order to find the fused report, $R^f = \{P^f(o_i)\}$, a cost function is defined such that it measures the discrepancy between the fusion result and each sensor report,

$$R^f = \min_r \sum_{l=1}^L w^l \cdot dist(r, R^l), \quad (1)$$

where, w^l determines the contribution of the l^{th} sensor report towards the fused report, and $dist(A, B)$ is a distance function measuring the discrepancy between the distributions A and B . In [5], Kulback-Liebler distance is used as the distance measure.

2) Dissimilar Sensor Fusion: The Dissimilar Sensor Fusion model makes the assumption that all sensors observe dissimilar characteristics of the target, and hence each sensor provides new information about the target. An additional sensor in this case generates increased resolution on the target identity. The cost function is then formulated such that the solution leads to a fusion report representing an enhanced resolution on the target identity, given the individual sensor reports. The

optimization problem to be solved is,

$$\begin{aligned} P^f = \min_p \sum_{l=1}^L w^l \sum_{i=1}^I \frac{1}{P^l(o_i)} p(o_i) - \sum_{i=1}^I \ln(p(o_i)) \\ \text{subject to: } \sum_{i=1}^I p(o_i) = 1, \quad p(o_i) \geq 0. \end{aligned} \quad (2)$$

These two models should be viewed as “extreme cases” of decision level fusion. There are many practical cases in which the sensors are neither completely similar nor completely dissimilar. Event Driven Fusion [8], [9] addresses this limitation and is discussed below.

B. Event Driven Fusion

Event Driven Fusion looks at fusion under a different light, by combining occurrences of events to reach a probability measure for target identity. Each sensor is said to make a decision on the occurrence of certain events that it is capable of observing, rather than making a decision on the target identity. This technique also explores the extent of dependence between features being observed by the sensors, and hence generates more informed probability distributions over the events.

Consider the set of objects/targets, $O = \{o_1, o_2, \dots, o_I\}$. Let the k^{th} feature from the l^{th} sensor be F_k^l . Then, a mutually exclusive set of events, $\Omega_k^l = \{a_{kj}^l\}_{j=1, \dots, J_{kl}}$, is defined over the feature F_k^l . Here, a_{kj}^l is the j^{th} event on F_k^l and is described as $a_{kj}^l : F_k^l \in [u_j, v_j]$, $u_j \in \mathbb{R}^+$, $v_j \in \mathbb{R}^+$, and $v_j > u_j$. A probability report is generated by the l^{th} sensor for each of its features, $R_k^l = \{\Omega_k^l, \sigma_B(\Omega_k^l), P_k^l\}$. An object/target is then defined as, $o_i \in \sigma_B(\Omega)$, where, $\Omega = \Omega_1^1 \times \dots \times \Omega_k^l \times \dots \times \Omega_{K_L}^L$. The joint probability in the product space is determined as a convex combination of the distributions with minimal mutual information and the one with maximal mutual information. For events $\gamma_k^l \in \sigma_B(\Omega_k^l)$

$$\begin{aligned} P_\Omega(\gamma_1^1, \dots, \gamma_k^l, \dots, \gamma_{K_L}^L) = \rho \cdot P_{\Omega_{\text{MAXMI}}}(\gamma_1^1, \dots, \gamma_k^l, \dots, \gamma_{K_L}^L) + \\ (1 - \rho) \cdot P_{\Omega_{\text{MINMI}}}(\gamma_1^1, \dots, \gamma_k^l, \dots, \gamma_{K_L}^L), \end{aligned} \quad (3)$$

where, $\rho \in [0, 1]$ is a pseudo-measure of correlation between the features. $\rho \approx 1$ when the features are highly correlated, and $\rho = 0$ when they are independent. For any object defined as a combination of events in the product space Ω , $o_i \in \sigma_B(\Omega)$, rules of probability can then be used to determine the object probability. For instance, in a 2-D scenario, an object may be defined as a combination of events $\gamma_1 \in \sigma_B(\Omega_1)$, and $\gamma_2 \in \sigma_B(\Omega_2)$. The combination defined in the product space, $\Omega = \Omega_1 \times \Omega_2$, may be of the form $o : \{\gamma_1 \wedge \gamma_2\}$ or $o : \{\gamma_1 \vee \gamma_2\}$. Given the joint probability, P_Ω , rules of probability can be used to determine the fused object probability as follows:

- $o : \{\gamma_1 \wedge \gamma_2\} : P^f(o) = P_\Omega(\gamma_1, \gamma_2)$
- $o : \{\gamma_1 \vee \gamma_2\} : P^f(o) = P_1(\gamma_1) + P_2(\gamma_2) - P_\Omega(\gamma_1, \gamma_2)$

Where, $P_1(\gamma_1)$ and $P_2(\gamma_2)$ are the marginal probabilities for detection of the events γ_1 and γ_2 as seen by sensors 1 and 2.

C. Generative Adversarial Networks

The Adversarial Network was first introduced by Goodfellow et al. [18] in 2014. In this framework, a generative model

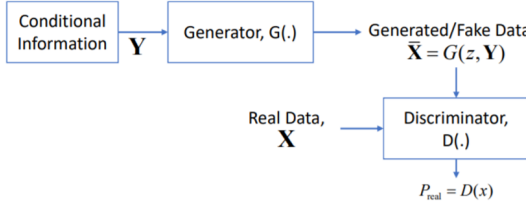


Fig. 1: Conditional Generative Adversarial Networks

is pitted against an adversary: the discriminator. The generator aims to confuse discriminator by synthesizing realistic samples from some underlying distribution. The discriminator on the other hand attempts to differentiate between a real data sample and that generated by the generator. Both these models are approximated by neural networks. When trained alternatively, the generator learns to produce random samples from the data distribution which are very close to the real data samples. Following this, Conditional Generative Adversarial Networks (CGANs) were proposed in [19]. These networks were trained to generate realistic samples from a class conditional distribution, by replacing the random noise input to the generator by some useful information (see Figure 1). Hence, the objective of the generator now became to generate realistic data samples, given the conditional information. CGANs have been used to generate random faces, given the facial attributes [20] and also to produce relevant images given text descriptions [21].

III. PROBLEM FORMULATION

Consider L sensors surveilling an area of interest. We wish to detect/recognize targets, $O = \{o_1, o_2, \dots, o_I\}$, given the data collected by the sensors. Let the n^{th} observation from the l^{th} sensor be denoted by, $x_n^l = \{x_{n_q}^l\}_{q=1 \dots d_l}$. Let $\mathbf{X}_{d_l \times N}^l = \{x_n^l\}_{n=1 \dots N}$ be the set of N observations made by the l^{th} sensor.

We consider the existence of a hidden space, $\mathbf{H}_{d_H \times N}$, between the L sensors. This hidden space may comprise of some features that are shared between the sensors, and some that are private to specific sensors. Under the assumption that such a hidden space exists, each sensor may select the optimal set of features for classification via a selection matrix, \mathbf{S}^l ,

$$\forall l \in \{1, \dots, L\}, \quad \mathbf{F}_{d_H \times N}^l = \mathbf{S}_{d_H \times d_H}^l \mathbf{H}_{d_H \times N}. \quad (4)$$

Since the hidden space represents the information shared by the sensors, there must also exist a mapping, $\mathbf{G}^l : \mathbf{X}^l \rightarrow \mathbf{H}$ such that,

$$\forall l \in \{1, \dots, L\}, \quad \hat{\mathbf{H}}_{d_H \times N}^l = \mathbf{G}^l(\mathbf{X}_{d_l \times N}^l) \approx \mathbf{H}_{d_H \times N} \quad (5)$$

From Equations 4 and 5 we have,

$$\forall l \in \{1, \dots, L\}, \quad \mathbf{F}_{d_H \times N}^l = \mathbf{S}_{d_H \times d_H}^l [(\mathbf{G}^l(\mathbf{X}^l))_{d_H \times N}]. \quad (6)$$

The existence of such a hidden space makes it possible to detect damaged sensors, and safeguard the system performance against them. When the l^{th} sensor is damaged, representative

features for that sensor are reconstructed from the hidden space via the selection operator, $\mathbf{F}^l = \mathbf{S}^l \mathbf{H}$. Following this, a linear classifier, $c_i^l(\mathbf{F}^l) = w_i^{l^T} \mathbf{F}^l + b_i^l$, is used to determine the classification score for the i^{th} object as seen by the l^{th} sensor. The probability of occurrence of that object is then determined as,

$$P^l(o_i^l) = \frac{\exp(w_i^{l^T} \mathbf{F}^l + b_i^l)}{\sum_{m=1}^L \exp(w_m^{l^T} \mathbf{F}^l + b_m^l)}. \quad (7)$$

Finally, given these probability reports, $R^l = \{P^l(o_i^l)\}$, the objective is to determine the fused probability report $R^f = \{P^f(o_i)\}$, which is achieved using a special case of Event Driven Fusion [8], [9].

IV. PROPOSED APPROACH

As discussed in the previous section, the hidden space, \mathbf{H} , can be estimated from the l^{th} sensor observations as, $\hat{\mathbf{H}}^l = \mathbf{G}^l(\mathbf{X}^l)$. The mapping \mathbf{G}^l is approximated by a neural network and is realized as the generator of a Conditional Generative Adversarial Network (CGAN), that generates the estimate of the hidden space, $\hat{\mathbf{H}}^l$, while conditioned on the observations of the l^{th} sensor. Hence, we will have L generators that generate L estimates of the hidden space.

The desired output of these generators is to generate the estimate, $\hat{\mathbf{H}}^l$, such that, $\forall l \in \{1, \dots, L\}$, $\hat{\mathbf{H}}^l = \mathbf{G}^l(\mathbf{X}^l) \approx \mathbf{H}$. On the other hand, the discriminator attempts to correctly identify the modality that the estimate of the hidden space was generated from. That is, it assigns a score, $D^l(\hat{h})$, which represents the probability that an estimate of the hidden space, \hat{h} , fed into the discriminator, \mathbf{D} , was generated by the l^{th} generator, \mathbf{G}^l . When updating the parameters for the l^{th} generator, the hidden space estimates generated by all the other generators are assumed to be the target space, and the l^{th} generator attempts to replicate these spaces, while at the same time attempting to generate an estimate that confuses the discriminator.

The standard formulation for the Generative Adversarial Network [18], [19] is known to have some instability issues [29]. Specifically, if the supports of the estimated hidden spaces are disjoint, which is highly likely when the inputs to the generators are coming from different modalities, a perfect discriminator is easily learned, and gradients for updating the generator may vanish. This issue was addressed in [29], and solved by using a Wasserstein GAN. So, using the sensor observations as the conditional information in the WGAN formulation [29], we have,

$$\begin{aligned} & \min_{\mathbf{G}^l} \max_{\mathbf{D}} \sum_{l=1}^L V(\mathbf{G}^l, \mathbf{D}), \\ & V(\mathbf{G}^l, \mathbf{D}) = \sum_{\substack{m=1 \\ m \neq l}}^L \{ \mathbb{E}_{\mathbf{G}^m(x^m) \sim \mathbb{P}_{\mathbf{H}}} [D^m(\mathbf{G}^m(x^m))] \\ & \quad - \mathbb{E}_{x^l \sim \mathbb{P}_{\mathbf{X}^l}} [D^l(\mathbf{G}^l(x^l))]\}. \end{aligned} \quad (8)$$

The discriminator, \mathbf{D} , in the above formulation is required to be compact and K-Lipschitz. This is done by clamping the weights of the discriminator to a fixed box (eg. $\theta_d \in$

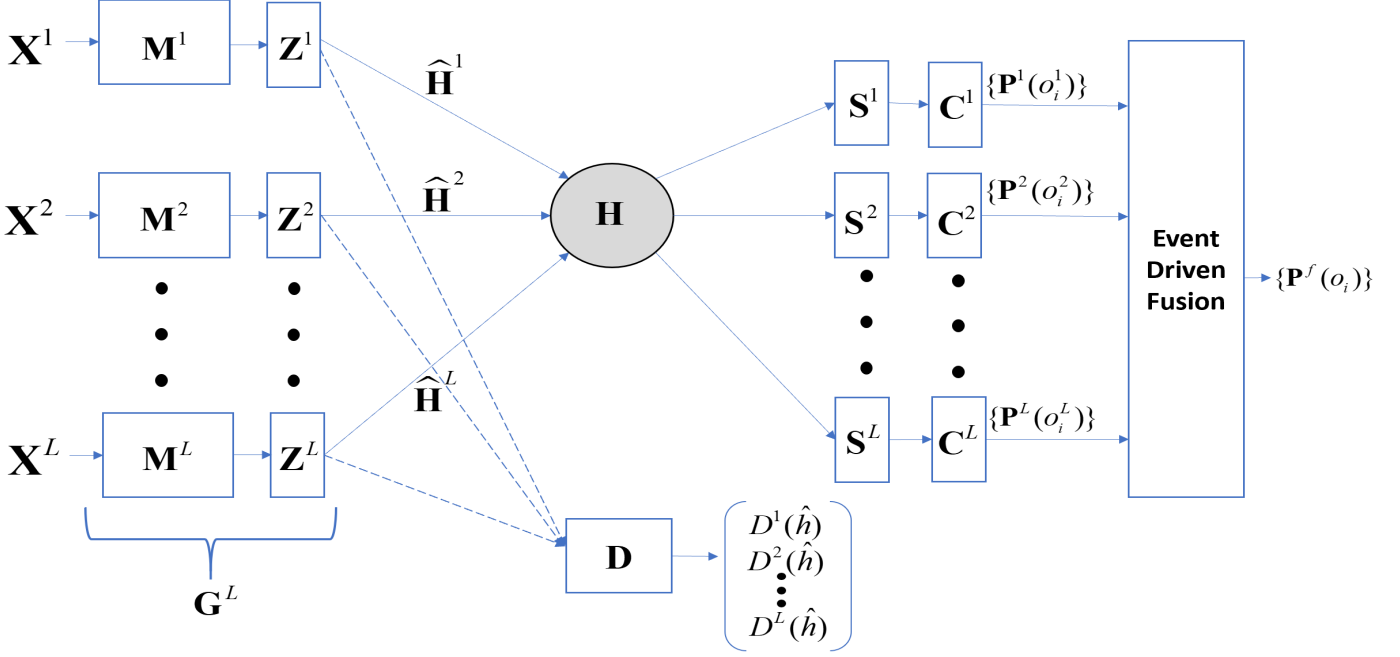


Fig. 2: Block diagram of the proposed approach for sensor fusion

$[-0.01, 0.01]$) [29]. The discriminator is updated once after every generator update. That is, for L sensors, the discriminator is updated L times for one update to the l^{th} generator (see Algorithm 1). While this causes the estimates to be close to each other, it does not guarantee that the generated hidden spaces share the same basis.

A similar idea toward finding a common representation between multiple modalities was very recently proposed in [28]. In this paper the authors attempt to find a common latent space between text and image modalities in order to perform image/text retrieval. Given a query from the image modality, the image is transformed into the latent common space, and the text with closest representation is retrieved.

In our work, we additionally ensure that the hidden space estimates share a common basis, leading to them lying in a common subspace. These hidden estimates are later used in order to detect damage in sensors based on how easily they can be clustered together, hence, it is important that they lie in a common subspace. In order to achieve this we enforce commutation between the operators that are responsible for transforming the data into the common subspace.

Definition 1. Linear operators $\mathbf{A} \in \mathbb{R}^{n \times n}$ and $\mathbf{B} \in \mathbb{R}^{n \times n}$ are said to commute if,

$$[\mathbf{A}, \mathbf{B}] = \mathbf{AB} - \mathbf{BA} = 0. \quad (9)$$

Theorem 1. If $\mathbf{A} \in \mathbb{R}^{n \times n}$ and $\mathbf{B} \in \mathbb{R}^{n \times n}$ are commuting linear operators, they share common eigenvectors.

Proof. Consider an eigenbasis of \mathbf{A} , $\mathcal{V} = \{v_i\}$, with λ_i the eigenvalue associated to v_i . Then for any v_i ,

$$\mathbf{AB}v_i = \mathbf{BA}v_i = \lambda_i \mathbf{B}v_i, \quad (10)$$

i.e., if $\mathbf{B}v_i \neq 0$, $\mathbf{B}v_i$ is an eigenvector of \mathbf{A} , associated to the

same eigenvalue as v_i , λ_i . \square

Theorem 2. If $\mathbf{A} \in \mathbb{R}^{n \times n}$ and $\mathbf{B} \in \mathbb{R}^{n \times n}$ are commuting operators that are also individually diagonalizable, they share a common eigenbasis.

Proof. If \mathbf{A} and \mathbf{B} are individually diagonalizable, they have n -distinct eigenvalues, i.e. \mathbf{A} can be diagonalized as, $\mathbf{A} = \mathbf{P}\mathbf{D}_A\mathbf{P}^{-1}$, where, \mathbf{D}_A is an $n \times n$ diagonal matrix with eigenvalues of \mathbf{A} on the diagonal and \mathbf{P} is an $n \times n$ matrix which has eigenvectors of \mathbf{A} as its columns. Since, both \mathbf{A} and \mathbf{B} share common eigenvectors (as seen in Theorem 1), \mathbf{B} can also be diagonalized as $\mathbf{B} = \mathbf{P}\mathbf{D}_B\mathbf{P}^{-1}$. Hence, \mathbf{A} and \mathbf{B} share a common eigenbasis. \square

Let \mathbf{G}^l be composed of a Convolutional Neural Network, \mathbf{M}^l , followed by a fully connected layer, \mathbf{Z}^l . Note that the fully connected layer does not have any non-linear activation, and acts as a linear transform on $\mathbf{M}^l(\mathbf{X}^l)$. So, now we have,

$$\hat{\mathbf{H}}^l = \mathbf{Z}_{d_H \times d_H}^l [\mathbf{M}^l(\mathbf{X}^l)]_{d_H \times N}. \quad (11)$$

If the operators $\mathbf{Z}^1, \dots, \mathbf{Z}^L$ commute, they will share a common eigenbasis. Furthermore, since the transformation, $\mathbf{Z}^l[\mathbf{M}^l(\mathbf{X}^l)]$ lies in the range space of the operator, \mathbf{Z}^l , $\forall l, \hat{\mathbf{H}}^l = \mathbf{Z}^l[\mathbf{M}^l(\mathbf{X}^l)]$ lie in a common subspace, due to the shared basis. Commutation cannot be guaranteed, but by including a penalty term in the optimization, we can encourage the operators to commute, hence leading to operators that are ‘almost commuting’. Note that \mathbf{Z}^l must be a square matrix in order to be able to compute the commutation cost as per Equation 9. On including this with the GAN loss, Equation 8

becomes,

$$\min_{\mathbf{G}^l, \mathbf{Z}^l} \max_{\mathbf{D}} \sum_{l=1}^L \{V(\mathbf{G}^l, \mathbf{D}) + \gamma_2 \sum_{\substack{m=1 \\ m \neq l}}^L \|\mathbf{Z}^l, \mathbf{Z}^m\|^2\} \quad (12)$$

Although the CGAN network is expected to eventually generate samples that lie in the same subspace as the target data, even without this auxiliary loss, we observe that the addition of this loss significantly helps the generator, especially since a target space is not clearly defined. Experiments show that including the commutation term speeds up convergence, and also leads to closer hidden space estimates.

A. Structure of the Hidden Space/Selection Operators

In addition to ensuring that the hidden space estimates generated by different modalities lie in a common subspace, it is also important to structure the hidden space in a way that it not only contains information shared between the sensor modalities, but also contains private information of individual modalities. This is important especially for heterogeneous sensors as they may provide additional information along with some common information. This conforms with the notion that no two sensors are completely similar or dissimilar. This is equivalent to structuring \mathbf{S}^l such that it selects features that are relevant to the l^{th} modality, while ignoring others. Such a structure can be achieved by encouraging the columns of the selection matrix to be close to zero. If the m^{th} column of \mathbf{S}^l is zeroed out, then the m^{th} feature in the hidden space, \mathbf{H} , does not contribute toward the l^{th} modality. This allows us to find the latent space, \mathbf{H} , that naturally separates information shared between different modalities from that private to each modality. We implement this by minimizing the $L_{\infty,1}$ norm, i.e., $\min_{\mathbf{S}^l} \|\mathbf{S}^l\|_{\infty,1}$, where,

$$\|\mathbf{S}^l\|_{\infty,1} = \sum_j \max_i (|s_{ij}^l|). \quad (13)$$

This minimizes the sum of the maximum of each column in \mathbf{S}^l . On adding this term to the generator cost function, we get,

$$\begin{aligned} \min_{\mathbf{G}^l, \mathbf{S}^l, \mathbf{Z}^l} \max_{\mathbf{D}} \sum_{l=1}^L & \{V(\mathbf{G}^l, \mathbf{D}) + \gamma_1 \|\mathbf{S}^l\|_{\infty,1} \\ & + \gamma_2 \sum_{\substack{m=1 \\ m \neq l}}^L \|\mathbf{Z}^l, \mathbf{Z}^m\|^2\} \end{aligned} \quad (14)$$

Notice that the above formulation has a trivial solution of setting $\mathbf{S}^l = \mathbf{0}$, and, $\mathbf{Z}^l = \mathbf{0}$ for all l . In order to avoid this solution, we also optimize the classification based on the selected features, \mathbf{F}^l , for each modality, via the minimization of the cross-entropy loss. This ensures that the learned features, \mathbf{F}^l , are optimal for object detection/recognition, which is only possible if $\mathbf{S}^l \neq \mathbf{0}$, and, $\mathbf{Z}^l \neq \mathbf{0}$. Given the sensor observations, \mathbf{X}^l , and the classifier $\mathbf{C}^l = \{c_i^l\}$, the cross-entropy loss is computed as,

$$C_{LOSS}^l(\mathbf{F}^l) = \sum_{n=1}^N \sum_{i=1}^I -y_{ni} \log \sigma(c_i^l(\mathbf{f}_n^l)), \quad (15)$$

where, $Y_n = \{y_{ni}\}$ is the ground truth for the n^{th} sample, σ is the soft-max function, and, $\mathbf{f}_n^l = \mathbf{S}^l[\mathbf{G}^l(\mathbf{x}_n^l)]$.

Finally, the optimization task is,

$$\begin{aligned} \min_{\mathbf{G}^l, \mathbf{Z}^l, \mathbf{S}^l, \mathbf{C}^l} \max_{\mathbf{D}} & \mathcal{L}(\mathbf{G}^l, \mathbf{D}, \mathbf{Z}^l, \mathbf{S}^l, \mathbf{C}^l) \\ \mathcal{L}(\mathbf{G}^l, \mathbf{D}, \mathbf{Z}^l, \mathbf{S}^l, \mathbf{C}^l) = & \sum_{l=1}^L \{V(\mathbf{G}^l, \mathbf{D}) + \gamma_1 \|\mathbf{S}^l\|_{\infty,1} \\ & + \gamma_2 \sum_{\substack{m=1 \\ m \neq l}}^L \|\mathbf{Z}^l, \mathbf{Z}^m\|^2 + \gamma_3 C_{LOSS}^l(\mathbf{F}^l)\}, \end{aligned} \quad (16)$$

where, γ_1 , γ_2 , and γ_3 are hyper-parameters that control the contribution of different terms toward the optimization.

The updates applied in order to train these networks are summarized in Algorithm 1. This setup learns the optimal features for classification, \mathbf{F}^l , while driven by the existence of the hidden space, \mathbf{H} , such that, $\mathbf{F}^l = \mathbf{S}^l \mathbf{H}$. Due to the inclusion of the selection matrix, \mathbf{S}^l , followed by the Classification Layer, we no longer require hand-crafting of features like in [8], [9]. The features of interest are learned and selected by the system during the training phase. The effects of the different terms in Equation 16 on the determined hidden spaces are shown in Section V-B in Figures 7, 8, and 9.

B. Special Case of Event Driven Fusion

In order to fuse the individual decisions from the sensors we use a special case of Event Driven Fusion. Instead of defining feature events for each object as in [8], an event in this case is the occurrence of the i^{th} object as seen by the l^{th} sensor, o_i^l . The l^{th} classifier, $\mathbf{C}^l = \{c_i^l\}$, provides the corresponding probability given the test sample, \mathbf{x}_t^l , $P_t^l(o_i^l) = \frac{\exp(c_i^l(\mathbf{f}_t^l))}{\sum_{m=1}^I \exp(c_m^l(\mathbf{f}_t^l))}$, as previously discussed in Section III. Each sensor report is now represented as, $R_t^l = \{P_t^l(o_i^l)\}$, and the fused probability of occurrence of the i^{th} object as per the rules of Event Driven Fusion [8] is determined as,

$$\begin{aligned} P_t^f(o_i) = P_t(o_i^1, o_i^2, \dots, o_i^L) &= \rho \cdot P_{\text{MAX MI}}(o_i^1, o_i^2, \dots, o_i^L) \\ &+ (1 - \rho) \cdot P_{\text{MIN MI}}(o_i^1, o_i^2, \dots, o_i^L), \end{aligned} \quad (22)$$

where ρ is a pseudo-measure of correlation between the sensor modalities. For making an informed decision in favor of an object, this formulation assumes all the modalities to be equally reliable. This is not always true in practical scenarios as certain sensors may provide more discriminative information as compared to others, and hence are more reliable. Due to this reason, it is important to assign a Degree of Confidence (DoC) in the decisions made by each sensor. The DoC in the decisions made by the l^{th} sensor given the test sample, \mathbf{x}_t^l , is defined as, $DoC_t^l \in [0, 1]$, where $DoC_t^l = 0$ implies that the sensor observations do not provide any useful information about the target identity, and $DoC_t^l = 1$ implies that information provided by the sensor is highly discriminative with respect to target classification. The individual sensor reports, $R_t^l = \{P_t^l(o_i^l)\}$, are now redefined as,

$$R_t^l = \{P_t^l(o_1^l), P_t^l(o_2^l), \dots, P_t^l(o_I^l), P_t^l(\text{unc}^l)\}, \quad (23)$$

Algorithm 1: Training the CGAN system

Let $\{\theta_{g_l}^q\}_{q \in \{1, \dots, Q\}}$ be the parameters for the q^{th} layer of the l^{th} generator, and \mathbf{y}_q be the output of that layer.

$\mathbf{y}^Q = \mathbf{Z}^l[\mathbf{M}^l(\mathbf{X}^l)]$, and, $\mathbf{y}^{Q-1} = \mathbf{M}^l(\mathbf{X}^l)$.

Similarly, Let $\{\theta_d^r\}_{r \in \{1, \dots, R\}}$ be the parameters of the r^{th} layer of the discriminator and \mathbf{z}^r be the output of that layer.

- for j in 1 : Number of Iterations

- for l in 1 : L

- * Update the discriminator network,

$$\theta_d^{r(j)} \leftarrow \theta_d^{r(j-1)} + \mu_D \left\{ \frac{d\mathcal{L}(\mathbf{G}^l, \mathbf{D}, \mathbf{Z}^l, \mathbf{S}^l, \mathbf{C}^l)}{d\mathbf{z}^R} \frac{d\mathbf{z}^R}{d\mathbf{z}^{R-1}} \dots \frac{d\mathbf{z}^{r+1}}{d\theta_d^r} \right\} \quad (17)$$

- * Update the l^{th} generator network,

$$\mathbf{C}^{l(j)} \leftarrow \mathbf{C}^{l(j-1)} - \mu_G \left\{ \frac{d\mathcal{L}(\mathbf{G}^l, \mathbf{D}, \mathbf{Z}^l, \mathbf{S}^l, \mathbf{C}^l)}{d\mathbf{C}^l} \right\} \quad (18)$$

$$\mathbf{S}^{l(j)} \leftarrow \mathbf{S}^{l(j-1)} - \mu_G \left\{ \frac{d\mathcal{L}(\mathbf{G}^l, \mathbf{D}, \mathbf{Z}^l, \mathbf{S}^l, \mathbf{C}^l)}{d\mathbf{C}^l(\mathbf{F}^l)} \frac{d\mathbf{C}^l(\mathbf{F}^l)}{d\mathbf{F}^l} \frac{d\mathbf{F}^l}{\mathbf{S}^l} + \frac{d\mathcal{L}(\mathbf{G}^l, \mathbf{D}, \mathbf{Z}^l, \mathbf{S}^l, \mathbf{C}^l)}{d\mathbf{S}^l} \right\} \quad (19)$$

$$\begin{aligned} \mathbf{Z}^{l(j)} &\leftarrow \mathbf{Z}^{l(j-1)} - \mu_G \left\{ \frac{d\mathcal{L}(\mathbf{G}^l, \mathbf{D}, \mathbf{Z}^l, \mathbf{S}^l, \mathbf{C}^l)}{d\mathbf{C}^l(\mathbf{F}^l)} \frac{d\mathbf{S}^l(\mathbf{Z}^l[\mathbf{M}^l(\mathbf{X}^l)])}{d\mathbf{Z}^l[\mathbf{M}^l(\mathbf{X}^l)]} \frac{d\mathbf{C}^l(\mathbf{F}^l)}{d\mathbf{F}^l} \frac{d\mathbf{Z}^l[\mathbf{M}^l(\mathbf{X}^l)]}{d\mathbf{Z}^l} + \frac{d\mathcal{L}(\mathbf{G}^l, \mathbf{D}, \mathbf{Z}^l, \mathbf{S}^l, \mathbf{C}^l)}{d\mathbf{Z}^l} \right\} \\ \theta_{g_l}^{q(j)} &\leftarrow \theta_{g_l}^{q(j-1)} - \mu_G \left\{ \frac{d\mathcal{L}(\mathbf{G}^l, \mathbf{D}, \mathbf{Z}^l, \mathbf{S}^l, \mathbf{C}^l)}{d\mathbf{C}^l(\mathbf{F}^l)} \frac{d\mathbf{C}^l(\mathbf{F}^l)}{d\mathbf{F}^l} \frac{d\mathbf{S}^l(\mathbf{G}^l(\mathbf{X}^l))}{d\mathbf{G}^l(\mathbf{X}^l)} \frac{d\mathbf{G}^l(\mathbf{X}^l)}{d\mathbf{y}^{Q-1}} + \frac{d\mathcal{L}(\mathbf{G}^l, \mathbf{D}, \mathbf{Z}^l, \mathbf{S}^l, \mathbf{C}^l)}{d\mathbf{G}^l(\mathbf{X}^l)} \frac{d\mathbf{G}^l(\mathbf{X}^l)}{d\mathbf{y}^{Q-1}} \right\} \left\{ \frac{d\mathbf{y}^{Q-1}}{d\mathbf{y}^{Q-2}} \dots \frac{d\mathbf{y}^{q+1}}{d\theta_{g_l}^q} \right\} \end{aligned} \quad (20)$$

$$\theta_{g_l}^{q(j)} \leftarrow \theta_{g_l}^{q(j-1)} - \mu_G \left\{ \frac{d\mathcal{L}(\mathbf{G}^l, \mathbf{D}, \mathbf{Z}^l, \mathbf{S}^l, \mathbf{C}^l)}{d\mathbf{C}^l(\mathbf{F}^l)} \frac{d\mathbf{C}^l(\mathbf{F}^l)}{d\mathbf{F}^l} \frac{d\mathbf{S}^l(\mathbf{G}^l(\mathbf{X}^l))}{d\mathbf{G}^l(\mathbf{X}^l)} \frac{d\mathbf{G}^l(\mathbf{X}^l)}{d\mathbf{y}^{Q-1}} + \frac{d\mathcal{L}(\mathbf{G}^l, \mathbf{D}, \mathbf{Z}^l, \mathbf{S}^l, \mathbf{C}^l)}{d\mathbf{G}^l(\mathbf{X}^l)} \frac{d\mathbf{G}^l(\mathbf{X}^l)}{d\mathbf{y}^{Q-1}} \right\} \left\{ \frac{d\mathbf{y}^{Q-1}}{d\mathbf{y}^{Q-2}} \dots \frac{d\mathbf{y}^{q+1}}{d\theta_{g_l}^q} \right\} \quad (21)$$

where, $P_t^l(o_i^l) = DoC_t^l * P_t^l(o_i^l)$, and $P_t^l(unc^l) = 1 - DoC_t^l$ is the probability that the l^{th} sensor is uncertain about the target identity. The joint probability distribution for the new sensor reports is now determined as,

$$\begin{aligned} P_t(a^1, a^2, \dots, a^L) &= \rho \cdot P_{\text{MAX MI}}(a^1, a^2, \dots, a^L) \\ &\quad + (1 - \rho) \cdot P_{\text{MIN MI}}(a^1, a^2, \dots, a^L), \end{aligned} \quad (24)$$

where, $a^l \in \{o_i^l, o_2^l, \dots, o_I^l, unc^l\}$, and the probability of occurrence of the i^{th} target is computed as,

$$\begin{aligned} P_t^f(o_i) &= P_t\left(\left(\bigwedge_{l=1}^L o_i^l\right) \bigvee_{m_1=1}^L (unc^{m_1} \bigwedge_{\substack{l=1 \\ l \neq m_1}}^L o_i^l) \right. \\ &\quad \left. \bigvee_{m_1, m_2=1}^L (unc^{m_1} \wedge unc^{m_2} \bigwedge_{\substack{l=1 \\ l \neq m_1 \\ l \neq m_2}}^L o_i^l) \right. \\ &\quad \left. \dots \bigvee_{m_1, m_{L-1}=1}^L \left(\bigwedge_{j=1}^{L-1} unc^{m_j} \bigwedge_{\substack{l=1 \\ \forall j, l \neq m_j}}^L o_i^l \right) \right), \end{aligned} \quad (25)$$

with a degree of confidence, $DoC_t^f = 1 - P_t(\bigwedge_{l=1}^L unc^l)$, in the fused decision.

For a 2D scenario (i.e. two sensors), the probability of occurrence of the i^{th} target is,

$$P_t^f(o_i) = P_t((o_i^1 \wedge o_i^2) \vee (unc^1 \wedge o_i^2) \vee (o_i^1 \wedge unc^2)), \quad (26)$$

with a degree of confidence, $DoC^f = 1 - P(unc^1 \wedge unc^2)$, in the fused decision. This formulation takes into account the potential uncertainties in the decisions made by individual sensors. Figure 3 shows the joint distribution to be determined in a 2D case.

The degree of confidence in the l^{th} sensor for classification

D_t^1	D_t^2	$DoC_t^1 P_t^2(o_i^2)$	$DoC_t^2 P_t^2(o_i^2)$	$P_t^2(unc^2)$
$DoC_t^1 P_t^1(o_i^1)$	$P(o_i^1, o_i^2)$	$P(o_i^1, unc^2)$	$P(o_i^1, unc^2)$	
$DoC_t^1 P_t^1(o_2^1)$	$P(o_2^1, o_i^2)$	$P(o_2^1, unc^2)$	$P(o_2^1, unc^2)$	
$P_t^1(unc^1)$	$P(unc^1, o_i^2)$	$P(unc^1, o_2^2)$	$P(unc^1, unc^2)$	

Fig. 3: Joint distribution for a 2D case, on including the probability of uncertainty. The joint distribution is determined following the rules of Event Driven Fusion.

of the test sample, \mathbf{x}_t^l , is determined as,

$$DoC_t^l = (1 - p_D(\hat{\mathbf{h}}_t^l)) \cdot Acc_{train}^l, \quad (27)$$

where, $p_D(\hat{\mathbf{h}}_t^l)$ is the probability of damage for the l^{th} sensor given the test sample, \mathbf{x}_t^l (discussed in detail in the next subsection), and Acc_{train}^l is the training accuracy of the l^{th} sensor. The training accuracy in Equation 27 represents prior information about the discrimination power of the sensor, while $(1 - p_D(\hat{\mathbf{h}}_t^l))$ represents the sensor condition at the time of implementation.

C. Detecting Damaged Sensors

Since \mathbf{H} is designed such that it is common for all the sensors, it may be used to detect a damaged sensor.

1) *Comparison Across Modalities*: The estimate, $\hat{\mathbf{H}}^m$, based on erroneous observations will significantly deviate from the estimates from normal observations (i.e. sensors that are not damaged), $\hat{\mathbf{H}}^l, l \neq m$. This allows detection of damage in a sensor during the implementation phase. The m^{th} sensor

is said to be damaged if,

$$\forall j, l \neq m, \sum_{\substack{l=1 \\ l \neq m}}^L \mathcal{I}(\|\hat{h}_t^m - \hat{h}_t^l\|^2 > T) \geq \begin{cases} \frac{L-1}{2}, & \text{if } L \text{ is odd,} \\ \frac{L}{2} - 1, & \text{if } L \text{ is even.} \end{cases}$$

$$\text{And, } \sum_{\substack{j,l=1 \\ j,l \neq m}}^L \mathcal{I}(\|\hat{h}_t^j - \hat{h}_t^l\|^2 < T) \geq \begin{cases} \frac{L-1}{2}, & \text{if } L \text{ is odd,} \\ \frac{L}{2} - 1, & \text{if } L \text{ is even.} \end{cases} \quad (28)$$

where, $\mathcal{I}(\cdot)$ is the indicator function, T is a threshold value determined from the training data, and \hat{h}_t^l is the estimated hidden space given the observation x_t^l . The limitation with this kind of an approach is that we can only detect up to $\frac{L-1}{2} / \frac{L}{2} - 1$ damaged sensors.

2) *Hierarchical Clustering*: A faulty sensor can also be detected by comparing the hidden space generated by the test sample with that generated from training data. One way to do this is by clustering normal sensor observations (from training data), and checking whether the hidden space estimate generated by the test sample can be assigned to one of these clusters. The concatenation of the training data, $\hat{\mathbf{H}}_{d \times LN}^C = \{\hat{\mathbf{H}}^1, \hat{\mathbf{H}}^2, \dots, \hat{\mathbf{H}}^L\}$, is first used to construct a clustering tree based on an Agglomerative approach (see Algorithm 2). The probability of the l^{th} sensor being damaged is then computed as,

$$p_D(\hat{h}_t^l) = \frac{d_{lev}}{\max_v d_v}, \quad (29)$$

where, d_v is the cut-off distance at clustering level v , and,

$$\begin{aligned} lev &= \arg \min v \\ s.t. \exists j &\in \{1, \dots, J_{lev}\}, \hat{h}_t^l \in Z_{lev}^j, \end{aligned} \quad (30)$$

$v = 1, \dots, V$ are the clustering levels, J_v is the number of clusters at level v , and Z_v^j is the j^{th} cluster at level v . This is a measure of how quickly the hidden space estimate, \hat{h}_t^l , can be clustered with the training data.

The l^{th} sensor is said to be damaged if,

$$p_D(\hat{h}_t^l) > T, \quad (31)$$

where, T , is a threshold value which will depend on the dataset, types of sensors, SNR, etc. In our implementation, we compute the optimal thresholds at different SNRs for the training data, and these thresholds are later used during the testing phase in order to determine whether a sensor is damaged or not. This probability measure is also used in Equation 27, in order to adapt the DoC based on the sensor condition during implementation. If the sensor is damaged, the representative features are generated using the selection matrix as,

$$\hat{f}_t^l = S^l \left(\frac{\sum_{m \in \Gamma} DoC_t^m \cdot \hat{h}_t^m}{\sum_{m \in \Gamma} DoC_t^m} \right), \quad (32)$$

where, Γ is the set of working sensors.

Algorithm 2: Hierarchical Clustering (Agglomerative Clustering)

- Initialize clusters at $v = 0$: $\mathcal{C}_0 = \{Z_0^j = \{h_j\}, j = 1 \dots L.N\}$
- while Number of Clusters > 1:
 - $v = v + 1$
 - Among all cluster pairs, $\{Z_{v-1}^r, Z_{v-1}^s\}$, find the one, say $\{Z_{v-1}^i, Z_{v-1}^j\}$, such that:

$$d(Z_{v-1}^i, Z_{v-1}^j) = \min_{r,s} d(Z_{v-1}^r, Z_{v-1}^s), \quad (33)$$

where, $d(\cdot)$ is a measure of dissimilarity.

- Assign $Z_v^q = Z_{v-1}^i \cup Z_{v-1}^j$
- Get new clustering: $\mathcal{C}_v = \{(\mathcal{C}_{v-1} - \{Z_{v-1}^i, Z_{v-1}^j\}) \cup Z_v^q\}$

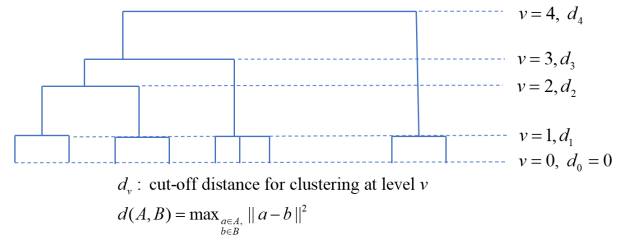
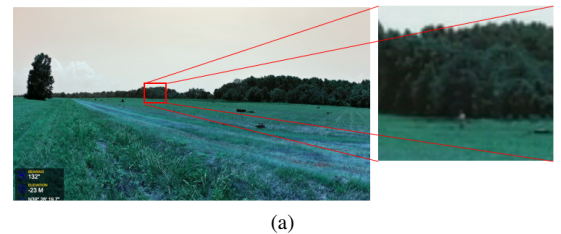


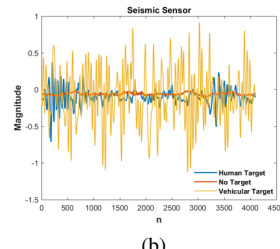
Fig. 4: A clustering tree created using Hierarchical Clustering (Agglomerative Clustering)

V. EXPERIMENTS AND RESULTS

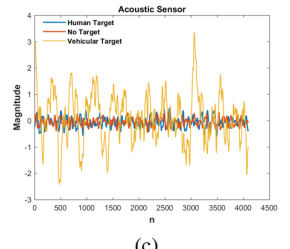
We validate our approach by running experiments on two different datasets. The first dataset we use is pre-collected



(a)



(b)



(c)

Fig. 5: (a): Sample video frame with a human target, (b): Sample seismic sensor observations for human target, vehicular target, and no target cases, (c): Sample acoustic sensor observations for human target, vehicular target, and no target cases.

data from a network of seismic, acoustic, and imaging sensors deployed in a field, where people/vehicles were walking/driven around in specified patterns. Details about this sensor setup

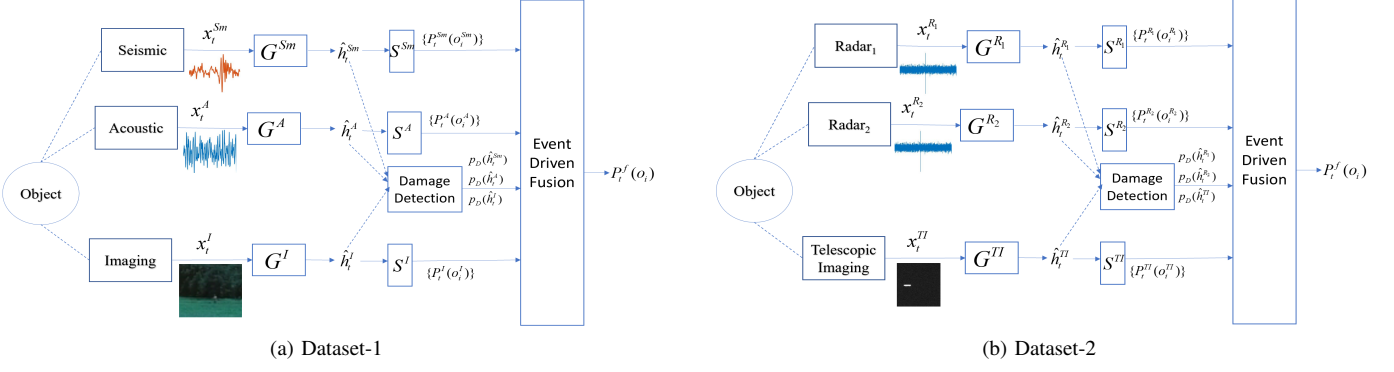


Fig. 6: Block Diagram of Implementation

and experiments can be found in [23]. This dataset has been previously used for target detection in [8], [13], [24], [25]. Here, we use this dataset to classify between human targets, vehicular targets, and no targets. Some data samples from the sensors can be seen in Figure 5. This will be referred to as ‘Dataset-1’ in the following discussions.

For our second experiment, we select two sensors, namely a Radar sensor and a telescopic optical sensor, for one (latter) of which we have acquired real data. For technical difficulty, our Radar measurements were never co-measured with the optical data. Both the sensors are ideally synchronized when observing a given target, which in our case, can be any object in outer space, such as satellite or space debris. For the radar simulations we use MATLAB Simulink, and for telescopic imaging we use images collected by the Czech Technical University in Prague. Each generated radar signal over one second is correlated with two telescopic images. Samples for objects with different velocities, cross-sections, ranges, and aspect-ratios are then generated.

Object classes are defined in the same way as in [9], based on events on the feature values. Note that these events are no longer required for training purposes, and are only used for the purposes of labeling the data. For the radar, we use the features, velocity (v), cross-section (cs), and range (r), and the events are defined as,

$$\begin{aligned} a_1^v : 0 \leq v \leq 10 \text{ m/s}, \quad a_2^v : 15 \text{ m/s} \leq v \leq 35 \text{ m/s}, \\ a_1^r : 0 < r \leq 300 \text{ m}, \quad a_2^r : 300 \text{ m} < r, \\ a_1^{cs} : 0 < cs \leq 20 \text{ m}^2, \quad a_2^{cs} : 15 \text{ m}^2 \leq cs \leq 50 \text{ m}^2. \end{aligned} \quad (34)$$

From the telescopic imaging sensor, the features, displacement (d) and aspect ratio (AR) define the following events,

$$\begin{aligned} a_1^d : 0 \leq d \leq 60 \text{ pixels}, \quad a_2^d : 90 \text{ pixels} \leq d \leq 210 \text{ pixels}, \\ a_1^{ar} : 0 < AR \leq 1.5, \quad a_2^{ar} : 1.5 < AR. \end{aligned} \quad (35)$$

Furthermore, the objects for classification are defined in terms of these events as,

$$o_1 : \{a_1^r \wedge [(a_2^v \wedge a_2^d) \vee (a_2^{cs} \vee a_2^{ar})]\} \quad (36)$$

$$o_2 : \{a_1^v \wedge a_1^d \wedge a_2^r \wedge a_1^{cs} \wedge a_1^{ar}\} \quad (37)$$

This will be referred to as ‘Dataset-2’ in the following discussions.

and discussions.

A. Implementation Details

Figure 6-(a) shows the block diagram for implementation of the discussed approach on Dataset-1. We no longer require handcrafted features and event definitions as in [8], [9], since we let the generative structure (see Figure 6) guide the learning of features. Similarly, the block diagram for implementation of this system on Dataset-2 can be seen in Figure 6-(b). The output of the l^{th} generator, G^l , for a test sample, x_t^l , is a d_H -dimensional estimate of the hidden space, \hat{h}_t^l . This hidden space is also used to detect potential damages to the sensors deployed. Following this the optimal features, f_t^l , are selected by each sensor for making decisions on target identities via the selection matrix, S^l . The decisions are then fed into the fusion system and a fused decision is made based on the rules discussed in Section IV-B.

The generator network uses 1-D convolutions in case of seismic/acoustic and radar modalities, and 2-D convolutions in case of the imaging sensors. We use a 6 layered Neural Network, with 2×2 max pooling layer after the 2^{nd} and 4^{th} layer. ReLU activation is used after each layer, except the max pooling layers. The first 4 layers are convolutional, while the last two are fully connected. The first two convolutional layers use a filter size of 5 and the next two use filter size 3. The first fully connected layer is used to transform the output of the convolutional layers into a d_H dimensional representation. All the layers preceding the final fully connected layer approximate the mapping M^l , while the final layer approximates the operator Z^l , and transforms the data into a common subspace.

For determining the dimension of the hidden space, we search over values ranging from $d = 50$ to $d = 5000$. For Dataset-1 we find the best performance at $d = 500$, while for Dataset-2, $d = 700$. In both cases we observe that at best performance, $d \ll d_l$.

B. Performance Analysis

Table I shows the performance of different techniques as compared with the proposed approach of using a Generative Adversarial Network to learn optimal features, which are then used for target detection. All sensors are assumed to

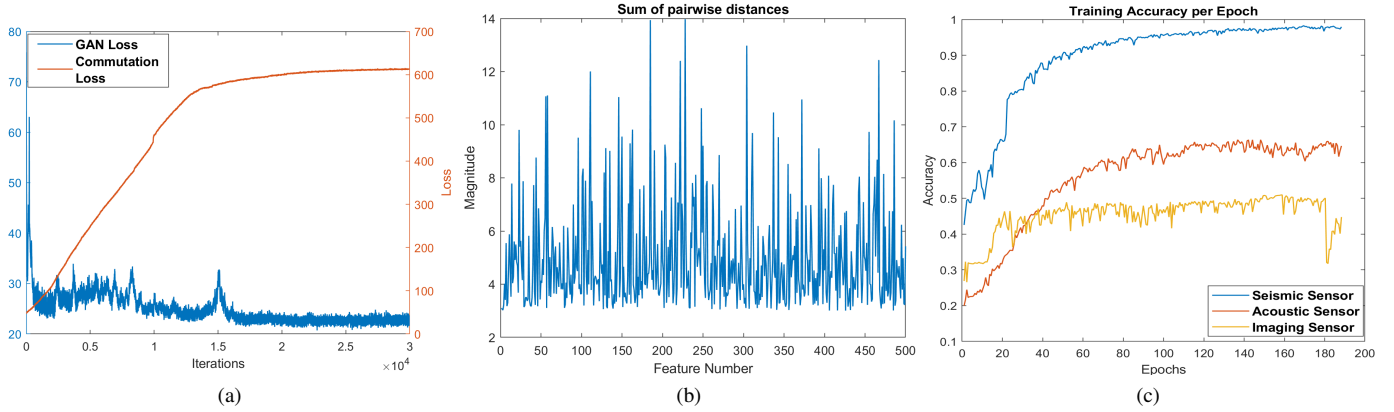


Fig. 7: (a): Optimization Losses, (b): Sum of pairwise distances between hidden estimates, (c): Training Accuracies/Epoch when GAN Loss is optimized in tandem with classification loss

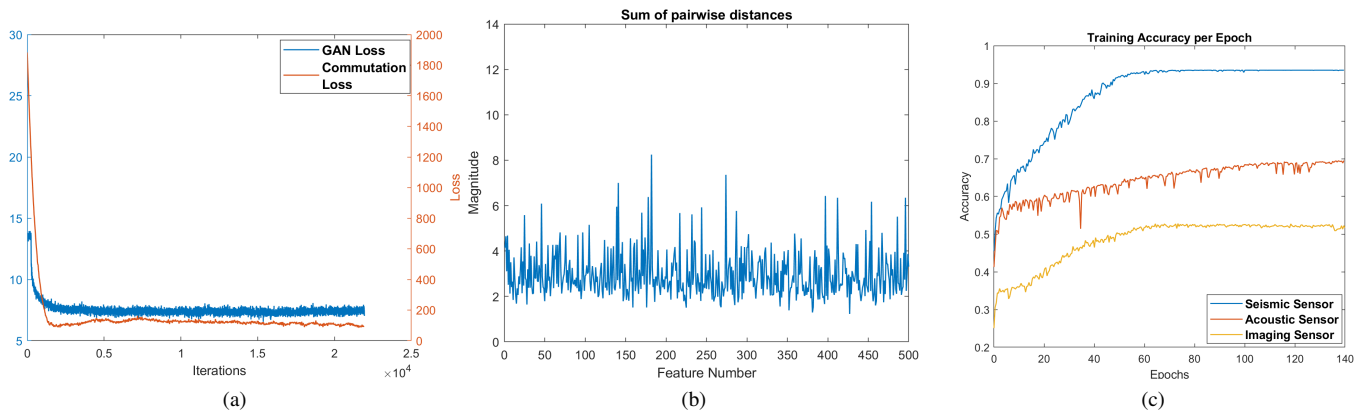


Fig. 8: (a): Optimization Losses, (b): Sum of pairwise distances between hidden estimates, (c): Training Accuracies/Epoch when commutation term is included with the GAN and classification term

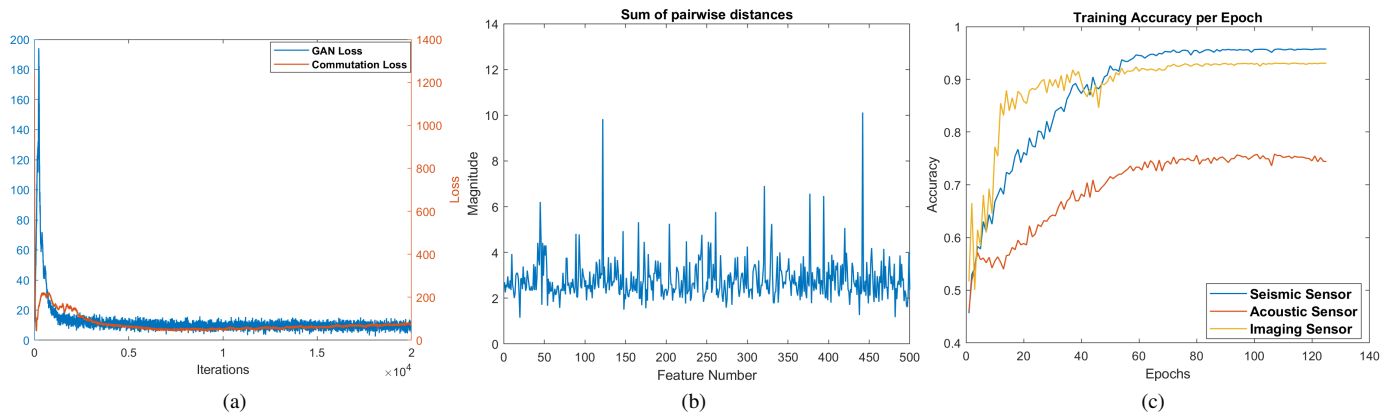
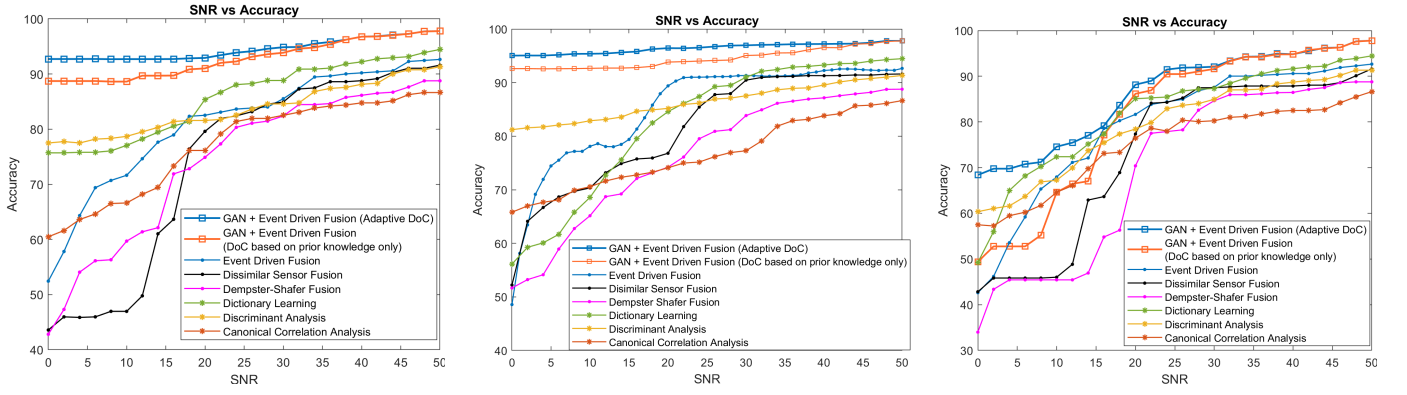


Fig. 9: (a): Optimization Losses, (b): Sum of pairwise distances between hidden estimates, (c): Training Accuracies/Epoch when all terms in Equation 16 are active.

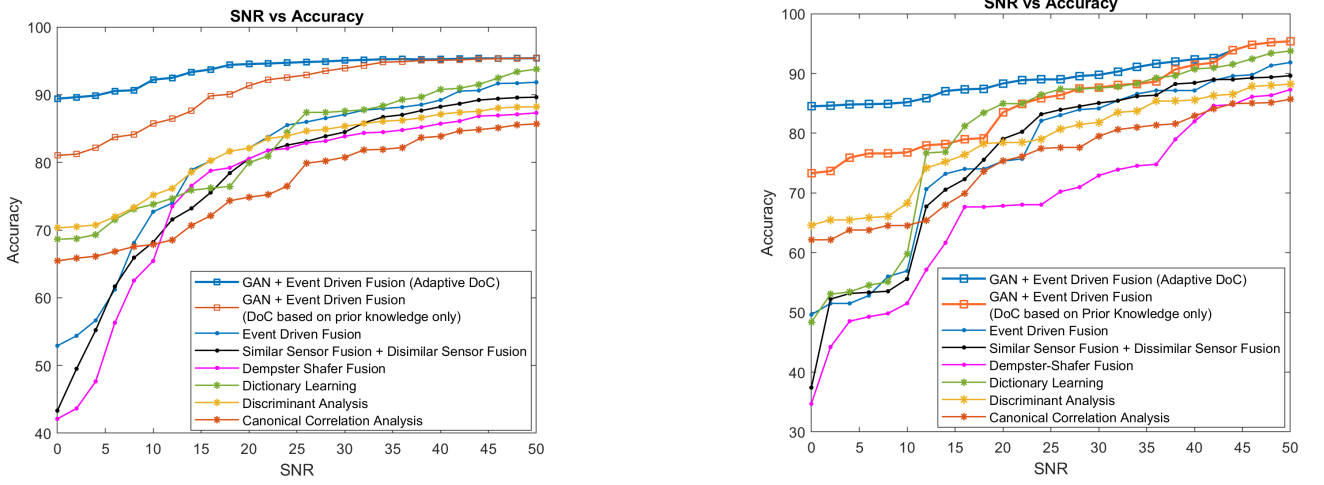


(a) Gaussian noise is added to Seismic and Acoustic Sensor, while Imaging data is assumed to be clean.

(b) Gaussian noise is added to Imaging and Acoustic Sensor, while Seismic data is assumed to be clean.

(c) Gaussian noise is added to Seismic and Imaging Sensor, while Acoustic data is assumed to be clean.

Fig. 10: Comparison of the proposed technique (GAN + Event Driven Fusion) with existing techniques for Dataset-1.



(a) Gaussian noise is added to the Telescopic Imaging Sensor, while Radar data is assumed to be clean.

(b) Gaussian noise is added to the Radar Sensors, while Telescopic Imaging data is assumed to be clean.

Fig. 11: Comparison of the proposed technique (GAN + Event Driven Fusion) with existing techniques for Dataset-2.

be working normally in Table I. Comparisons are made with approaches that perform fusion on the decision level, as well as those that seek a hidden space for fusion. We find that using the individual sensor features (whose learning is driven by the existence of a structured hidden space) for classification and performing decision level fusion on these classifications leads to better performance compared to trying to classify based on the hidden space directly. For the evaluation of Model Based Fusion approaches (see Section II-A), the dissimilar sensor setting is considered for Dataset-1 as all three sensors are different. On the other hand, for Dataset-2, the two radars are first combined using similar sensor fusion and the result of this is combined with the telescopic sensor using dissimilar sensor fusion.

We also compare the effects of different losses in our objective. First we implement a system which uses the Adversarial setup, along with the classification loss, i.e., γ_1 , and γ_2 in Equation 16 are set to 0. The losses are seen in Figure 7-

(a). The blue plot represents the negative of the discriminator loss for the GAN network (y-axis on left), while orange plot corresponds to the commutation loss (y-axis on right). Figure 7-(b) shows the sum of pairwise distances between the hidden estimates generated by the three sensors, i.e. $\text{Magnitude}(k) = \sum_{l,m=1}^L (\mathbf{H}^l(k) - \mathbf{H}^m(k))^2$, where, $k \in \{1, \dots, d_H\}$, refers to the feature number in the d_H -dimensional hidden space. Figure 7-(c) shows the individual classification performance of the sensors. It is observed that the performance of Seismic and Acoustic Sensors improves as the model is updated, but the performance of the imaging sensor is very low.

Figure 8 shows the optimization losses when the commutation term is added to the objective, i.e. only γ_1 is set to zero in Equation 16. This leads to minimization of the pairwise commutation loss, hence forcing the hidden space estimates to lie in a common subspace. It is seen that including the commutation cost leads to closer hidden spaces (Figure 8-(b)). Although, the performance of the imaging sensor is still not

TABLE I: Performance Comparison for the First Dataset

Method	Accuracy (Dataset-1)	Accuracy (Dataset-2)
Seismic Sensor	93.62 %	-
Acoustic Sensor	68.71 %	-
Imaging Sensor	90.33 %	-
Radar Sensor 1	-	89.33 %
Radar Sensor 2	-	86.73 %
Telescopic Imaging Sensor	-	83.57 %
Feature Concatenation	88.13 %	86.45 %
Dissimilar Sensor Fusion	91.61 %	-
Similar + Dissimilar Sensor Fusion	-	89.63 %
Dempster-Shafer Fusion	88.77 %	87.30 %
Event Driven Fusion (Without using GAN structure) [8], [9]	92.04 %	90.36 %
Canonical Correlation Analysis [25]	86.64 %	85.69 %
Discriminant Analysis	91.33 %	88.21 %
Dictionary Learning [26]	94.46 %	93.77 %
Hidden Space Generated by GAN	95.13 %	91.13 %
Event Driven Fusion + GAN	97.79 %	95.34 %

increasing significantly.

Figure 9 shows the optimization loss when all the terms in Equation 16 are active. The imaging sensor now starts giving better performance. Since the $L_{\infty,1}$ norm on the selection matrix allows representation of private/shared features in the hidden space, the heterogeneity of the imaging sensor is maintained, and features selected are more optimal toward classification based on the imaging sensor. The effects of the $L_{\infty,1}$ norm can also be seen in the differences between the hidden estimates in Figure 9-(b), where now there are some features that have more difference compared to others, as they may correspond to private features.

C. Robustness Analysis

The major advantage of learning a hidden space between the modalities is the ability to detect sensor damage during implementation, and furthermore being able to generate representative features for that damaged sensor as seen in Equation 32. The contribution of the representative features towards the fused decision can also be controlled via the degree of confidence.

We also study how the performance of the system varies with different Signal to Noise Ratios. At a given time one sensor is assumed to be working normally, while noise is added to the other sensors.

Figures 10 and 11 show the degradation of the fusion performance as the SNR decreases for Dataset-1 and Dataset-2, respectively. The plots with ‘asterisk’(*) markers represent approaches that look for a common subspace in order to

fuse the different modalities, while those with ‘dot’(.) markers represent approaches that perform fusion at the decision level. Finally, the plots with ‘square’ markers show the performance of the proposed approach. The blue plot uses adaptive DoC ($DoC_t^l = (1 - p_D(\hat{h}_t^l)).Acc_{train}^l$), while the orange plot only uses the prior information ($DoC_t^l = Acc_{train}^l$), which is also the case for other plots using decision level fusion. It is observed that it is important to update the DoC during the implementation based on the sensor condition, rather than only depending on the prior information about the discriminative abilities of the sensor.

Furthermore, the above graphs show that the degradation has severe effects in the case where the seismic and imaging sensors are damaged. This is due to the fact that the discriminative power of the acoustic sensor is low, and in spite of adapting the DoC and generating representative features, the performance is limited by the information contained in the observations of the sensor. A similar trend is also observed for Dataset-2, where the telescopic imagery has lower discriminative ability compared to the radar sensors.

VI. CONCLUSION

In this paper, we proposed a data driven approach that learns a structured hidden space between the sensors via a Generative Adversarial Network. The hidden space is used to learn the features of interest for target classification. The hidden space serves a dual purpose as it can also be utilized to detect noisy/damaged sensors and take the required steps to remedy the situation. Experiments on multiple datasets show that the proposed approach is able to make the system robust to noisy/damaged sensors, and outperforms existing fusion algorithms.

REFERENCES

- [1] D. L. Hall and J. Llinas, An introduction to multisensor data fusion, Proceedings of the IEEE, vol. 85, no. 1, pp. 623, Jan 1997.
- [2] Bahador Khaleghi, Alaa Khamis, Fakhreddine O. Karray, and Saiedeh N. Razavi, Multisensor data fusion: A review of the state-of-the-art, Information Fusion, vol. 14, no. 1, pp. 28–44, 2013.
- [3] Arthur P Dempster, A generalization of bayesian inference., Classic works of the dempster-shafer theory of belief functions, vol. 219, pp. 73104, 2008.
- [4] Glenn Shafer et al., A mathematical theory of evidence, vol. 1, Princeton university press Princeton, 1976.
- [5] Lingjie Li, Data fusion and filtering for target tracking and identification, Ph.D. thesis, 2003.
- [6] Lingjie Li, Zhi-Quan Luo, Kon Max Wong, and Eloi Bosse, Convex optimization approach to identify fusion for multisensor target tracking, IEEE Transactions on Systems, Man, and Cybernetics-Part A: Systems and Humans, vol. 31, no. 3, pp. 172178, 2001.
- [7] Mihai Cristian Florea and Eloi Bosse, Critiques on some combination rules for probability theory based on optimization techniques, in Information Fusion, 2007 10th International Conference on. IEEE, 2007
- [8] Roheda, Siddharth, Hamid Krim, Zhi-Quan Luo, and Tianfu Wu. "Decision Level Fusion: An Event Driven Approach." In 2018 26th European Signal Processing Conference (EUSIPCO), pp. 2598-2602. IEEE, 2018.
- [9] Roheda, Siddharth, Hamid Krim, Zhi-Quan Luo, and Tianfu Wu. "Robust Event Driven Fusion." *In Press*
- [10] Judy Hoffman, Saurabh Gupta, and Trevor Darrell, Learning with side information through modality hallucination, in Proceedings of the IEEE Conference on Computer Vision and Pattern Recognition, 2016, pp. 826834.
- [11] Geoffrey Hinton, Oriol Vinyals, and Jeff Dean, Distilling the knowledge in a neural network, arXiv preprint arXiv:1503.02531, 2015.
- [12] Vladimir Vapnik and Rauf Izmilov, Learning using privileged information: similarity control and knowledge transfer., Journal of machine learning research, vol. 16, no. 20232049, pp. 55, 2015.
- [13] Siddharth Roheda, Benjamin S Riggan, Hamid Krim, and Liyi Dai, Cross-modality distillation: A case for conditional generative adversarial networks, in 2018 IEEE International Conference on Acoustics, Speech and Signal Processing (ICASSP). IEEE, 2018, pp. 29262930.
- [14] Sarah Rastegar, Mahdieh Soleymani, Hamid R Rabiee, and Seyed Mohsen Shojaei, Mdl-cw: A multimodal deep learning framework with cross weights, in Proceedings of the IEEE Conference on Computer Vision and Pattern Recognition, 2016, pp. 26012609.
- [15] Raghu Raman Gopalan, Ruonan Li, and Rama Chellappa, Domain adaptation for object recognition: An unsupervised approach, in Computer Vision (ICCV), 2011 IEEE International Conference on. IEEE, 2011, pp. 9991006.
- [16] Jingjing Zheng, Ming-Yu Liu, Rama Chellappa, and P Jonathon Phillips, A grassmann manifold-based domain adaptation approach, in Pattern Recognition (ICPR), 2012 21st International Conference on. IEEE, 2012, pp. 20952099.
- [17] Jie Ni, Qiang Qiu, and Rama Chellappa, Subspace interpolation via dictionary learning for unsupervised domain adaptation, in Proceedings of the IEEE Conference on Computer Vision and Pattern Recognition, 2013, pp. 692699.
- [18] Ian Goodfellow, Jean Pouget-Abadie, Mehdi Mirza, Bing Xu, David Warde-Farley, Sherjil Ozair, Aaron Courville, and Yoshua Bengio, Generative adversarial nets, in Advances in neural information processing systems, 2014, pp. 26722680.
- [19] Mehdi Mirza and Simon Osindero, Conditional generative adversarial nets, arXiv preprint arXiv:1411.1784, 2014.
- [20] Jon Gauthier, Conditional generative adversarial nets for convolutional face generation, Class Project for Stanford CS231N: Convolutional Neural Networks for Visual Recognition, Winter semester, vol. 2014, no. 5, pp. 2, 2014.
- [21] Scott Reed, Zeynep Akata, Xincheng Yan, Lajanugen Logeswaran, Bernt Schiele, and Honglak Lee, Generative adversarial text to image synthesis, arXiv preprint arXiv:1605.05396, 2016.
- [22] Phillip Isola, Jun-Yan Zhu, Tinghui Zhou, and Alexei A Efros, Image-to-image translation with conditional adversarial networks, arXiv preprint arXiv:1611.07004, 2016.
- [23] Sylvester M Nabritt, Thyagaraju Damarla, and Gary Chatters, Personnel and vehicle data collection at aberdeen proving ground (apg) and its distribution for research, Tech. Rep., ARMY RESEARCH LAB ADELPHI MD SENSORS AND ELECTRON DEVICES DIRECTORATE, 2015.
- [24] Kyunghun Lee, Benjamin S Riggan, and Shuvra S Bhattacharyya, An accumulative fusion architecture for discriminating people and vehicles using acoustic and seismic signals, in Acoustics, Speech and Signal Processing (ICASSP), 2017 IEEE International Conference on IEEE, 2017, pp. 29762980.
- [25] Iyengar, Satish G., Pramod K. Varshney, and Thyagaraju Damarla. "On the detection of footsteps based on acoustic and seismic sensing." In 2007 Conference Record of the Forty-First Asilomar Conference on Signals, Systems and Computers, pp. 2248-2252. IEEE, 2007.
- [26] Bahrampour, Soheil, Nasser M. Nasrabadi, Asok Ray, and William Kenneth Jenkins. "Multimodal task-driven dictionary learning for image classification." IEEE transactions on Image Processing 25, no. 1 (2016): 24-38.
- [27] Christian Szegedy, Vincent Vanhoucke, Sergey Ioffe, Jon Shlens, and Zbigniew Wojna, Rethinking the inception architecture for computer vision, in Proceedings of the IEEE Conference on Computer Vision and Pattern Recognition, 2016, pp. 28182826.
- [28] Peng, Yuxin, and Jinwei Qi. "Cm-gans: Cross-modal generative adversarial networks for common representation learning." ACM Transactions on Multimedia Computing, Communications, and Applications (TOMM) 15.1 (2019): 22.
- [29] Arjovsky, Martin, Soumith Chintala, and Léon Bottou. "Wasserstein gan." arXiv preprint arXiv:1701.07875 (2017).